Atmos. Chem. Phys. Discuss., 11, 23203–23229, 2011
www.atmos-chem-phys-discuss.net/11/23203/2011/
doi:10.5194/acpd-11-23203-2011

Atmospheric Chemistry and Physics Discussions

Hygroscopic behavior of individual $NaNO_3$ particles

M.-J. Lee, H.-J. Jung, H.-J. Eom, S. Maskey, H. K. Kim, and C.-U. Ro

Department of Chemistry, Inha University, Incheon, 402-751, Korea

Received: 9 August 2011 – Accepted: 15 August 2011 – Published: 17 August 2011

Correspondence to: C.-U. Ro (curo@inha.ac.kr)

Published by Copernicus Publications on behalf of the European Geosciences Union.

Abstract

Previous controversial studies on the hygroscopic behavior of $NaNO_3$ aerosols and our frequent observation of crystalline $NaNO_3$-containing ambient aerosol particles prompted this extensive hygroscopic study on $NaNO_3$ aerosol particles. In this work, the hygroscopic behavior of individual $NaNO_3$ particles of 2.5–4.0 µm in diameter is investigated on a single-particle basis using an optical microscopy technique. Quite different hygroscopic behaviors between particles generated by the nebulization of $NaNO_3$ solution and powdery particles were observed; i.e., most of generated particles continuously grew and shrank during humidifying and dehydration processes, respectively, and yet all the individual powdery particles had reproducible deliquescence and efflorescence relative humidities (DRHs and ERHs). The different behaviors of the two $NaNO_3$ systems are due to the different nucleation mechanisms. Our hygroscopic studies of $NaNO_3$ particles generated from aqueous $NaNO_3$ solutions indicate that they nucleate via homogeneous nucleation, but the time scale for the nucleation to occur is too long to be atmospherically relevant. And thus no efflorescence of the particles has been observed in the laboratory measurements. However, when chemical species acting as heterogeneous nuclei are present, then efflorescence occurs which can explain the observation of ambient crystalline $NaNO_3$ particles. It is imperative to work with heterogeneous nucleation systems which are more relevant to the real world.

1 Introduction

Sea-salt aerosol is one of the most abundant airborne particle types, especially in the coarse fraction (Keene et al., 1998). When "genuine" (or fresh) sea-salt aerosols, which are emitted by the so-called *bubble bursting* or *sea spray* process, react with various nitrogen oxides, such as HNO_3, N_2O_5, NO_2, and NO_3, in the atmosphere, sea-salts such as $NaNO_3$ can be formed, resulting in chlorine loss (Gibson et al., 2006). As the physicochemical properties of secondary $NaNO_3$ particles are different from those of NaCl

ACPD
11, 23203–23229, 2011

particles, the modified properties of the secondary aerosol particles can differently influence the climate through their modified direct radiative properties of scattering and absorbing incoming solar radiation and their modified effectiveness to serve as cloud condensation nuclei (indirect radiative forcing) (Jacobson, 2001; Hu et al., 2010). Also, it has been recognized that the hygroscopic properties of aerosol particles have played important roles in some heterogeneous reactions, e.g. the reaction of NaCl and $CaCO_3$ particles to form nitrate (Ten Brink, 1998; Krueger et al., 2003).

Since the understanding of the hygroscopic properties of airborne particles is important in the study of the physicochemical changes of aerosol particles, there have been many studies on the deliquescence and efflorescence behavior of aerosol particles (Tang, 1996; Tang and Fung, 1997; Tang and Munkelwitz, 1994; Tang et al., 1997; Cohen et al., 1987a, b, c; Weingartner et al., 2002; Gysel et al., 2002; Lee and Hsu, 1998, 2000; Ge et al., 1996, 1998; Martin, 2000; Ebert et al., 2002; Hoffman et al., 2004; Mikhailov et al., 2009). The sizes of hygroscopic particles in the atmosphere can vary depending on the ambient relative humidity (RH). In other words, particles can grow by absorbing water with the increase in RH (humidifying process), or shrink when water evaporates with the decrease in RH (dehydration process). For particles which deliquesce and effloresce during humidifying and dehydration processes, respectively, the size of dry particles remains unchanged with the increase in RH until the deliquescence RH (DRH) is reached. At their DRH, the solid particles become aqueous droplets, and they experience hygroscopic growth above the DRH. When RH is decreased, the concentration of salts in the aqueous droplets increases and the inorganic salts can crystallize at their efflorescence RH (ERH). It is also known that the ERH is sometimes significantly lower than the DRH, which is called hysteresis.

Up until now, the hygroscopic properties of $NaNO_3$ aerosol particles of micrometer size have been extensively studied. The first report on the hygroscopic properties of $NaNO_3$ particles appeared in 1994 where their DRH and ERH were listed as 74.5 % and 30–0.05 %, respectively, using a single-particle levitation technique, and it was briefly stated that the $NaNO_3$ solution droplets usually crystallized at RH = 20–30 %

ACPD
11, 23203–23229, 2011

(Tang and Munkelwitz, 1994). A charged single-particle of 14–16 µm in diameter obtained from a filtered $NaNO_3$ solution was injected into the single-particle levitation cell and the mass of a levitated solution droplet was determined at different RHs. Later, a full growth factor curve of a typical $NaNO_3$ particle was presented, showing distinctive DRH and ERH at 74.5 % and 35 %, respectively (Tang and Fung, 1997). Very recently, a study reported that an individual $NaNO_3$ aerosol of 1 µm size, generated by nebulization and deposited on a Si_3N_4 window, showed DRH and ERH at ~75 % and ~35 %, respectively, although just one measurement was performed using single-particle scanning transmission X-ray microscopy and NEXAFS and the experimental data points were somewhat sparse (Ghorai and Tivanski, 2010).

The first report on $NaNO_3$ particles without showing DRH and ERH appeared in 2000, where particles were generated by nebulization and subsequently collected on a Teflon filter, and then the liquid water contents of aerosols at different RHs were determined by an analyzer with a thermal conductivity detector (Lee and Hsu, 2000). Their humidograph showed continuous increases and decreases in the liquid water content during the humidifying and dehydration processes, respectively, without showing distinct DRH and ERH. Thereafter, many studies that have reported similar hygroscopic behavior of $NaNO_3$ aerosols, i.e. continuous growth and shrinkage during humidifying and dehydration processes, respectively, have appeared by the use of various types of analytical techniques such as a hygroscopicity tandem differential mobility analyzer (H-TDMA) (Gysel et al., 2002; Hu et al., 2010), environmental scanning electron microscopy (ESEM) (Hoffman et al., 2004), a multi-analysis aerosol reactor system (MAARS) (Gibson et al., 2006), attenuated total reflection FT-IR (Lu et al., 2008), and micro-FT-IR spectroscopy (Liu et al., 2008). These types of $NaNO_3$ aerosols were reported to be amorphous solids that were round in shape (Hoffman et al., 2004; Liu et al., 2008).

In the field, $NaNO_3$-containing ambient aerosol particles were quite often observed to be crystalline and angular, as shown in our previous works on the single-particle characterization of ambient aerosols (Hwang and Ro, 2006; Kang et al., 2009; Song

ACPD
11, 23203–23229, 2011

et al., 2010; Geng et al., 2011), strongly indicating that ambient $NaNO_3$ particles can be present in a crystalline, solid phase in the air, contrary to the prediction by most of the previous laboratory works. The controversial previous reports on the hygroscopic behavior of generated $NaNO_3$ particles and our frequent observation of crystalline ambient $NaNO_3$ aerosol particles led to our extensive investigation of the hygroscopic behavior of laboratory-generated from aqueous $NaNO_3$ solutions and powdery $NaNO_3$ particles, resulting in a clear explanation for the controversial reported results.

2 Experimental section

2.1 Particle samples

$NaNO_3$ powders of different purities (99.999 % and 98 %, Sigma-Aldrich) were used in this work. $NaNO_3$ particles of micrometer size were generated by the nebulization of aqueous $NaNO_3$ solutions onto 200 mesh Cu TEM grids coated with Formvar stabilized with carbon (Ted Pella, Inc.), Al foil (Sigma-Aldrich, 99.8 % purity, 0.05 mm thickness), or Ag foil (Goodfellow Inc., 99.95 % purity, 0.025 mm thickness). Hereafter, these particles generated by the nebulization of aqueous $NaNO_3$ solutions are termed as "generated $NaNO_3$ particles". For the nebulization, an atomizer (HCT4810, single jet atomizer) was used with N_2 (99.999 % purity) or ambient air. The solution droplets were dried by passing through a silica packed diffusion dryer (residence time of ca. 2 s, HCT4920 Diffusion dryer). Aqueous $NaNO_3$ solutions were made using ultrapure DI water (18 MΩ, Millipore Direct-Q^{TM}) or tap water. Powdery $NaNO_3$ samples were prepared by placing ground $NaNO_3$ powders on the TEM grids.

2.2 Hygroscopic property measurement

The hygroscopic behavior of aerosol particles was investigated at room temperature (23–25 °C) using a "see-through" inertia impactor apparatus equipped with an optical

ACPD
11, 23203–23229, 2011

microscope. The experimental set-up was described in our previous paper (Ahn et al., 2010). Briefly describing the set-up, the apparatus is composed of three parts: (A) the see-through impactor, (B) an optical microscope, and (C) a humidity controlling system. Collecting substrates, such as TEM grids and Al and Ag foils, on which either the generated $NaNO_3$ or powdery particles were deposited, were placed on the impaction plate in the see-through impactor. Dry N_2 gas was passed through a bubbler containing de-ionized (DI) water, allowing the N_2 to become saturated with water. The saturated and dry N_2 gases were mixed at different flow rates controlled by two mass flow controllers, resulting in a N_2 gas flow with controlled RH that went into the impactor. The RH, monitored by a digital hygrometer (Testo 645), varied from ~3 % to ~97 % in 0.1–0.3 % steps. The digital hygrometer was calibrated using a dew-point hygrometer (M2 Plus-RH, GE), resulting in RH readings within 0.3 % accuracy. The particles collected on the impact plate were seen through a nozzle throat by the use of an optical microscope (Olympus, BX51M). The images of particles were recorded using a digital camera (Canon EOS 5D, full frame, Canon EF f/3.5 L macro USM lens). The image size was 4368 ×2912 pixels and the image recording condition was set as ISO200. The exposure time was 0.4 s, and the DOF was F/3.5. In our study, the particle size was determined by measuring the particle area in the optical image. The optical images of the particles were processed using an image analyzing software (Matrox, Inspector v9.0). The size of an imaging pixel was calibrated using 10 µm Olympus scale bars, enabling the determination of a size change of 0.1 µm (equivalent to 4 pixels in the images). Particles with D_p>0.5 µm could be analyzed using this system. By increasing and decreasing RH, humidifying and dehydration curves, based on the size measurement of particles at each RH, were obtained for all individual particles seen within the optical image field. In order to achieve a steady state for condensing or evaporating water, each humidity condition was sustained for two minutes.

ACPD
11, 23203–23229, 2011

3 Results and discussion

3.1 Hygroscopic behavior of the generated $NaNO_3$ particles

Figure 1 shows several optical images of an image field of $NaNO_3$ particles deposited on a TEM grid by the nebulization of 1 M $NaNO_3$ aqueous solution using DI water, which were obtained at different RHs during humidifying and dehydration processes. It has been reported that all the generated $NaNO_3$ particles were round in shape under ESEM (Hoffman et al., 2004) and SEM (Liu et al., 2008). However, as shown in Fig. 1, seven and two particles happened to look round and angular, respectively, among nine aerosol particles on the image field, at RH = 3.4 % before the start of the first humidifying process (Fig. 1a). Among the two angular particles #2 and #3, only particle #3 effloresced to become angular again after the first dehydration process. In our study, the probability of encountering angular $NaNO_3$ was 4.5 % (16 among 358 individual particles generated by the nebulization of DI solution of $NaNO_3$ with N_2 gas, in the same way most of the other researchers had done; see Case 1 of Table 1). Among the 16 angular particles, just four effloresced to become angular again after the first dehydration process.

As the optical images were recorded using the digital camera by varying the RH in 0.1–0.3 % steps, growth factor curves for all of the aerosol particles in the image field during the humidifying and dehydration processes were obtained after the processing of the image data. Figure 2 shows the humidifying and dehydration data (displayed as blanks and solids, respectively) for round and angular $NaNO_3$ particles #1–3 in Fig. 1. The humidifying and dehydration data were obtained first by increasing RH from 3.4 % to 93.2 %, and then by decreasing RH to 3.5 %. Growth factors were obtained by dividing surface areas of the particles at different RHs by the surface area obtained at RH = 3.4 % before starting the humidifying process. The round particle #1, as well as the other round ones, continuously grew and shrank during the humidifying and dehydration processes, respectively, without distinct deliquescence and efflorescence. As shown in Fig. 2a, two repeated cycles of humidifying and dehydration processes,

ACPD
11, 23203–23229, 2011

and several further cycles, although not shown in Fig. 2a, produced almost identical curves. Herein, this type of particle is designated "type 1". All type 1 particles look round on their optical image at every RH.

The angular particles showed two different types of hygroscopic behavior during humidifying and dehydration cycles. The first type of angular particles deliquesced during the first hydration process, and yet they did not effloresce during the first dehydration process (*e.g.*, particle #2 in Fig. 1). In the following cycles, they just grew and shrank without deliquescence and efflorescence (Fig. 2b). Herein, this type of particles is designated "type 2". The other type showed clear and consistent DRHs and ERHs during the repeated cycles (e.g., particle #3; Fig. 2c). This type of particles is designated "type 3".

Table 1 shows the probabilities of encountering types 1–3 for nine different experimental cases. The first case (case 1) is for the $NaNO_3$ particles generated from DI solution of $NaNO_3$ of 99.999 % purity and deposited onto the TEM grid substrate. For case 1, the probabilities of encountering type 1–3 particles among 358 particles are 93.3 %, 5.6 %, and 1.1 %, respectively. Our observation on the hygroscopic behavior of type 1 particles is the same as those reported previously, in that the generated $NaNO_3$ particles looked round and continuously grew and shrank during hydration and dehydration processes (Hoffman et al., 2004; Liu et al., 2008). Although the probabilities of encountering type 2 and 3 particles are low, the DRHs of type 2 and 3 aerosols are 73.5–73.8 % and the ERHs of type 3 particles are 18.5–26.6 % (Table 2, case 1), which are close to the values (DRH = 74.5 % and ERH = 0.05–35 % (mostly 20–30 %)) reported by Tang and Munkelwitz (1994). We believe that Tang and Munkelwitz observed type 3 particles, whereas other studies have reported the hygroscopic behavior of type 1 $NaNO_3$ particles because of the absence of DRH and ERH. In our study, overall 358 individual particles were investigated and only four aerosol particles showed consistent DRHs and ERHs (type 3).

ACPD
11, 23203–23229, 2011

3.2 Hygroscopic behavior of $NaNO_3$ powdery particles

Hygroscopic measurements were performed for individual $NaNO_3$ powders of micrometer size which were put on TEM grids after grinding $NaNO_3$ powders purchased from Aldrich (99.999 % purity). Typical optical images taken at different RHs during the humidifying and dehydration processes are shown in Fig. 3, where all the particles on the image field showed clear deliquescence and efflorescence during humidifying and dehydration processes, respectively. Figure 4 shows the humidifying and dehydration data (displayed as blanks and solids, respectively) of a typical $NaNO_3$ powder (particle labeled 1 in Fig. 3) for the first and second cycles. During the first and second humidifying processes, the powdery particles clearly deliquesced at RH = 74.2 %, which is close to the reported DRH of $NaNO_3$ (Tang and Munkelwitz, 1994). During the first and second dehydration processes, the particle #1 effloresced at RH = 35.8 % and 37.0 %, respectively, which is somewhat higher than the reported ERH = 0.05–35 % (Tang and Munkelwitz, 1994). The DRH and ERH of 47 powdery individual particles were 74.0(±0.2) %, and in the range 26.7–45.3 %, respectively (Table 2, case 2). The ERH values for the individual generated and powdery particles were scattered compared to their DRH values. It is well known that aqueous inorganic droplets effloresce at somewhat different RHs as they contain different amounts of nucleation seeds in them and/or are located on surfaces with different roughnesses, acting like a nucleation seed (Han and Martin, 1999; Pant et al., 2006).

Up to now, just two brief reports on the hygroscopic properties of powdery $NaNO_3$ particles have been published; when a charged *solid* particle of 20 µm diameter was injected into a cubic electrodynamic levitation cell, distinctive DRH and ERH were observed at slightly greater than 70 % and below about 40 %, respectively (Lamb et al., 1996). Hoffman et al. (2004) performed a humidifying experiment on powdery $NaNO_3$ particles where deliquescence was clearly observed, although the dehydration process was not performed and the hydration process was performed just once. When $NaNO_3$ powders were exposed to RH = 85 % in the vacuum chamber of ESEM and then dried

ACPD
11, 23203–23229, 2011

under vacuum, they observed that particles larger than ~50 µm diameter effloresced, and yet particles of micrometer size did not. The authors suggested that the bigger particles had a higher chance of containing seed crystals inside the particles, which could act as heterogeneous nuclei for crystallization. Their observation is different from our observation, in that all the powdery particles of micrometer size (mostly in the diameter range 2.5–4.0 µm) showed clear and consistent deliquescence and efflorescence in several repeated cycles. As they also used $NaNO_3$ powders purchased from Aldrich (of similar purity to ours), the difference between their and our observations might be due to the difference between the substrates used, i.e. our TEM grids and their sticky carbon tape, indicating the presence of a substrate effect on the hygroscopic behavior of aerosol particles. We performed humidifying and dehydration experiments for powdery particles prepared on three different days and confirmed clear and consistent deliquescence and efflorescence of the powdery particles. Also, all the powdery $NaNO_3$ particles of 98 % purity showed clear DRHs and ERHs during repeated humidifying and dehydration processes (Table 1, case 3).

3.3 Why are hygroscopic behaviors of the generated and powdery $NaNO_3$ particles different?

The differences in hygroscopic behavior between the generated and powdery $NaNO_3$ particles seem to be mainly due to the presence of seed germs inside particles. Although the purity of commercial $NaNO_3$ powders is 99.999 %, our assumption is that commercial, crystalline powders must have been manufactured with the help of a trace amount of unrevealed seed germs. Taking into account the existence of the seed germs, all the powdery particles recrystallized during the dehydration process through a heterogeneous nucleation mechanism. When the commercial, crystalline powders were dissolved in DI water and particles were generated by the nebulization of the aqueous solutions using N_2 gas of 99.999 % purity, seed germs became absent in most of the generated particles, and then three types of particle were encountered in this study; (1) type 1 particles that looked round in shape were encountered with the

ACPD
11, 23203–23229, 2011

probability of 93.3 %, and showed no deliquescence and efflorescence, (2) type 2 particles are angular or round without seed germs (the encountering probability was 5.6 %), which only deliquesced in the first humidifying process, and (3) type 3 particles are angular crystalline with seed germs (the encountering probabilities was 1.1 %), which consistently deliquesced and effloresced in the repeated cycles. Hoffman et al. (2004) reported that the generated $NaNO_3$ particles were round, metastable, amorphous solid particles at very low RH, which continuously grew and shrank during humidifying and dehydration processes, respectively, showing the same behavior as the type 1 particles in this work. During the generation of $NaNO_3$ aerosol particles by nebulization, a small fraction of the generated particles were collected as angular crystalline particles either with or without seed germs that had been present in the commercial, crystalline powders.

Most of the previous experimental results and those shown here could be clearly explained with the help of additional experiments performed to validate this assumption:

1. DRH for the powdery particles (73.5–74.2 %) is the same as that for the generated type 2 and 3 particles (73.4–73.9 %), as the existence of the seed germs does not matter in deliquescence. However, the ERHs for the powdery particles (26.7–47.1 %) are higher than the values for the generated type 2 or 3 particles (either no ERH or ERH = 18.5–26.6 %, respectively). The generated type 2 particles do not contain seed germs and thus no efflorescence was observed. Although the generated type 3 particles contain seed germs in them, their amount and the effectiveness of the seed germs should be lower than for the powdery particles, which did not experience loss of their seed germs during dissolution in DI water, resulting in the lower ERHs of type 3 particles. Depending on the amount and effectiveness of seed germs, the ERHs of the powdery and type 3 particles varied widely in the range 18.5–47.1 %.

2. We let the generated 127 round $NaNO_3$ particles on TEM grids stay in the vacuum desiccator where RH = 15 %. Every 12 h, aerosol particles on each grid were

ACPD
11, 23203–23229, 2011

observed using an optical microscope, where the RH at the laboratory was kept below 60 %. After 3 days, a particle started to become angular in shape, resulting in 11 angular particles after 27 days. Just based on the morphology change, the time required for crystallization by homogeneous nucleation at RH = 15 % was at least 72 h, which is longer than the measurement times (at most several hours in other studies). Crystallization through homogeneous nucleation depends on the random process for the generation of seed germs (critical clusters), which could occur within a second or take longer than several months depending on chemical species and supersaturation (Martin, 2000). Figure 5 shows optical images of an exemplar image field where 13 generated round particles are seen. When the generated particles were put in a vacuum desiccator, particles #1–3 in Fig. 5 became angular after 3, 7, and 13 days, respectively, and no particles became angular thereafter. The angular particles, which had stayed for 27 days, showed clear DRH at 74.6 %, but no ERH. Indeed, overall 11 angular particles turned out to be type 2 aerosols, with clear DRHs and no ERHs for the first humidifying and dehydration processes, respectively, but without DRHs and ERHs for the further repeated cycles. Particles #4 and #5 look round, but they are also type 2 particles. Overall 68 of the round particles after 27 days in the desiccator appeared to be type 2 particles (see Table 1, case 4), indicating that homogeneous nucleation does not usually accompany the morphology change.

3. Liu et al. (2008) dried $NaNO_3$ aerosol particles generated by nebulization in an oven heated to ~100 °C overnight, and found that the oven-treated $NaNO_3$ particles looked angular in shape and XRD measurements confirmed their crystalline structure. When the oven-treated $NaNO_3$ particles underwent the first hydration process, they showed clear DRH at RH = 71–73 %, and yet no efflorescence was observed during the first dehydration process. This behavior is the same as what we observed for type 2 particles. We also dried $NaNO_3$ aerosol particles in a vacuum oven at ~110 °C overnight and observed type 1–3 particles for the oven-treated particles although the number of angular particles are small (nine among

ACPD
11, 23203–23229, 2011

overall 138 particles; Table 1, case 5). As the probabilities to encounter type 1–3 particles were 6.5 %, 86.2 %, and 7.3 %, respectively, showing that the majority of the oven-treated particles are type 2 particles, the heating did not usually change the morphology. The heating helped to convert the amorphous particles into crystalline ones through homogeneous crystallization, but without heterogeneous seed germs; the crystalline particles did not recrystallize during the dehydration process on the measurement time scale. The somewhat high probability of encountering type 3 particles might be due to contamination during the heating in the vacuum oven.

4. Another commercial $NaNO_3$ powder of lower purity (Aldrich, 98 % purity) was used for the generation of $NaNO_3$ particles by nebulization as it was expected that the powders would contain more seed germs than those of 99.999 % purity. Indeed, the probability of encountering type 3 particles was significantly enhanced to 3.6 % (eight among 224 generated particles; Table 1, case 6), that is 3 times more than that for the 99.999 % purity sample.

5. When particles were generated by nebulization of $NaNO_3$ solutions using DI water and N_2 gas, most seed germs that had been present in the powders seemed to be lost. In order to intentionally provide seed germs in the generated particles, tap water and ambient air instead of DI water and N_2 gas were used to generate $NaNO_3$ particles from the solution of $NaNO_3$ powders of 99.999 % purity. The probability of encountering type 3 particles was significantly enhanced to 6.6 % (nine among 137 generated particles; Table 1, case 7), that is 6 times more than that for ones generated using DI water and N_2 gas.

6. The rough surface of a collecting substrate was reported to act like a nucleation seed (Han and Martin, 1999; Pant et al., 2006), so that Al and Ag foils with rough surfaces were investigated as collecting substrates. When the particles were generated by nebulization of $NaNO_3$ solutions using DI water and N_2 gas, the observed numbers of type 2 and 3 particles were substantial; i.e. 20.0 % and

ACPD
11, 23203–23229, 2011

20.8 %, respectively, on Al foil and 8.3 % and 91.7 %, respectively, on Ag foil (Table 1, cases 8 and 9). As shown in Fig. 6, all the particles look angular on Ag foil, which has sharp grooves that act like effective nucleation seeds. Al foil also has grooves, but they seem to be less effective than those of Ag foil. As shown in Table 2, the DRHs of type 2 and 3 aerosols collected on Al and Ag foils are close to those on TEM grids, whereas the ERHs of type 3 aerosols are highest on Ag foil although the range of ERHs is also largest, indicating that the surface of the Ag foil is the most effective for inducing efflorescence of $NaNO_3$ particles. This substantial substrate effect on the efflorescence phenomenon needs to be further investigated.

7. In our hygroscopic measurement system employing an optical microscope, hygroscopic measurements can be done quickly and also the morphology of the particles at each RH is recorded. Therefore, it was possible to encounter type 3 particles when a significant number of generated particles were investigated in our work. Other previous studies seem to have worked with type 1 particles because of their high encountering probability. The observation of distinct DRH and ERH for generated $NaNO_3$ particles was reported only by Tang's group (Tang and Munkelwitz, 1994; Tang and Fung, 2007). In their work, relatively large aerosols of 14–16 µm size were investigated over a measurement time of several hours. The homogeneous nucleation rate is known to be faster for larger particles (Martin, 2000). In our study, the generated and powdery particles are those of 2.5–4.0 µm in diameter, which is an environmentally relevant size range. Therefore, it is probable that in the work of Tang's group the measurement time was long enough to observe the efflorescence of the larger aerosol particles. Also it was suggested that the bigger particles had a higher chance of containing seed crystals inside the particles, which could provide a template for the recrystallization (Hoffman, 2004).

ACPD
11, 23203–23229, 2011

4 Conclusions and summary

Previous controversial studies on the hygroscopic behavior of $NaNO_3$ aerosols and our frequent observation of crystalline $NaNO_3$-containing ambient aerosol particles prompted this extensive hygroscopic study on $NaNO_3$ aerosols. In this work, the hygroscopic behavior of individual $NaNO_3$ particles of 2.5–4.0 µm in diameter is investigated on a single-particle basis. Quite different hygroscopic behaviors between particles generated by the nebulization of $NaNO_3$ solution and powdery particles were observed; i.e., most of generated particles continuously grew and shrank during humidifying and dehydration processes, respectively, and yet all the individual powdery particles had reproducible deliquescence and efflorescence relative humidities (DRHs and ERHs). The different behaviors of the two $NaNO_3$ systems are due to the different nucleation mechanisms. Our hygroscopic studies of $NaNO_3$ particles generated from aqueous $NaNO_3$ solutions indicate that they nucleate via homogeneous nucleation, but the time scale for the nucleation to occur is too long to be atmospherically relevant. And thus no efflorescence of the particles has been observed in the laboratory measurements. However, when chemical species acting as heterogeneous nuclei are present, then efflorescence occurs. As the chemical company from which the $NaNO_3$ powders were purchased did not provide the information on crystal germs present in the powders, it is only speculated that the crystal germs might be insoluble solids. If they were soluble inorganic compounds, then they would be present homogeneously in aqueous solutions when the powders were dissolved in the water. And the generated $NaNO_3$ aerosol particles would contain the crystal germs acting as heterogeneous nuclei, resulting in type 3 particles. However, if the crystal germs were insoluble solids, then they would be present at a specific region in aqueous solutions due to their different density from the solutions, resulting in the smaller chance to be contained in the generated particles. As the hygroscopic studies of $NaNO_3$ aerosol particles based on the homogeneous nucleation mechanism turned out to provide results deviating from the phenomena happening in the real world, where $NaNO_3$-containing particles seem to

ACPD
11, 23203–23229, 2011

follow a heterogeneous nucleation mechanism due to the ample availability of chemical species acting as seed germs, it is imperative to work with heterogeneous nucleation systems.

Acknowledgements. This research was supported by the Basic Science Research Program through the National Research Foundation of Korea (NRF) funded by the Ministry of Education, Science and Technology (2010-0018881) and an Inha University Research Grant.

References

Ahn, K.-H., Kim, S.-M., Jung, H.-J., Lee, M.-J., Eom, H.-J., Maskey, S., and Ro, C.-U.: Combined use of optical and electron microscopic techniques for the measurement of hygroscopic property, chemical composition, and morphology of individual aerosol particles, Anal. Chem., 82, 7999–8009, 2010.

Cohen, M. D., Flagan, R. C., and Seinfeld, J. H.: Studies of concentrated electrolyte solutions using the electrodynamic balance. 1. Water activities for single-electrolyte solutions, J. Phys. Chem., 91, 4563–4574, 1987a.

Cohen, M. D., Flagan, R. C., and Seinfeld, J. H.: Studies of concentrated electrolyte solutions using the electrodynamic balance. 2. Water activities for mixed-electrolyte solutions, J. Phys. Chem., 91, 4575–4582, 1987b.

Cohen, M. D., Flagan, R. C., and Seinfeld, J. H.: Studies of concentrated electrolyte solutions using the electrodynamic balance. 3. Solute nucleation, J. Phys. Chem., 91, 4583–4590, 1987c.

Ebert, M., Inerle-Hof, M., and Weinbruch, S.: Environmental scanning electron microscopy as a new technique to determine the hygroscopic behaviour of individual aerosol particles, Atmos. Environ., 36, 5909–5916, 2002.

Ge, Z., Wexler, A. S., and Johnston, M. V.: Multicomponent Aerosol Crystallization, J. Colloid Interface Sci., 183, 68–77, 1996.

Ge, Z., Wexler, A. S., and Johnston, M. V.: Deliquescence Behavior of Multicomponent Aerosols, J. Phys. Chem., A 102, 173–180, 1998.

Geng, H., Ryu, J., Maskey, S., Jung, H.-J., and Ro, C.-U.: Characterisation of individual aerosol particles collected during a haze episode in Incheon, Korea using the quantitative ED-EPMA technique, Atmos. Chem. Phys., 11, 1327–1337, doi:10.5194/acp-11-1327-2011, 2011.

ACPD

11, 23203–23229, 2011

Gibson, E. R., Hudson, P. K., and Grassian, V. H.: Physicochemical Properties of Nitrate Aerosols: Implications for the Atmosphere, J. Phys. Chem. A, 110, 11785–11799, 2006.
Ghorai, S. and Tivanski, A. V.: Hygroscopic Behavior of Individual Submicrometer Particles Studied by X-ray Spectromicroscopy, Anal. Chem., 82, 9289–9298, 2010.
Gysel, M., Weingartner, E., and Baltensperger, U.: Hygroscopicity of Aerosol Particles at Low Temperatures. 2. Theoretical and Experimental Hygroscopic Properties of Laboratory Generated Aerosols, Environ. Sci. Technol., 36, 63–68, 2002.
Han, J. H. and Martin, S. T.: Heterogeneous nucleation of the efflorescence of $(NH_4)_2SO_4$ particles internally mixed with Al_2O_3, TiO_2, and ZrO_2, J. Geophys. Res., 104, 3543–3553, 1999.
Hoffman, R. C., Laskin, A., and Finlayson-Pitts, B. J.: Sodium nitrate particles: physical and chemical properties during hydration and dehydration, and implications for aged sea salt aerosols, J. Aerosol Sci., 35, 869–887, 2004.
Hu, D., Qiao, L., Chen, J., Ye, X., Yang, X., Cheng, T., and Fang, W.: Hygroscopicity of Inorganic Aerosols: Size and Relative Humidity Effects on the Growth Factor, Aerosol Air Qual. Res., 10, 255–264, 2010.
Hwang, H. and Ro, C.-U.: Direct observation of nitrate and sulfate formations from mineral dust and sea-salts using low-Z particle electron probe X-ray microanalysis, Atmos. Environ., 40, 3869–3880, 2006.
Jacobson, M. J.: Strong radiative heating due to the mixing state of black carbon in atmospheric aerosols, Nature, 409, 695–697, 2001.
Kang, S., Hwang, H., Kang, S., Park, Y., Kim, H., and Ro, C.-U.: Quantitative ED-EPMA combined with morphological information for the characterization of individual aerosol particles collected in Incheon, Korea, Atmos. Environ., 43, 3445–3453, 2009.
Keene, W. C., Sander, R., Pszenny, A. A. P., Vogt, R., Crutzen, P. J., and Galloway, J. N.: Aerosol pH in the marine boundary layer: A review and model evaluation, J. Aerosol Sci., 29, 339–356, 1998.
Krueger, B. J., Grassian, V. H., Iedema, M. J., Cowin, J. P., and Laskin, A.: Probing Heterogeneous Chemistry of Individual Atmospheric Particles Using Scanning Electron Microscopy and Energy-Dispersive X-ray Analysis, Anal. Chem., 75, 5170-5179, 2003.
Lamb., D., Moyle, A. M., and Brune, W. H.: The Environmental Control of Individual Aqueous Particles in a Cubic Electrodynamic Levitation System, Aerosol Sci. Technol., 24, 263–278, 1996.

ACPD
11, 23203–23229, 2011

Lee, C.-T. and Hsu, W.-C.: A novel method to measure aerosol water mass, J. Aerosol Sci., 29, 827–837, 1998.
Lee, C.-T. and Hsu, W.-C.: The measurement of liquid water mass associated with collected hygroscopic particles, J. Aerosol Sci., 31, 189–197, 2000.
Liu, Y., Yang, Z., Desyaterik, Y., Gassman, P. L., Wang, H., and Laskin, A.: Hygroscopic Behavior of Substrate-Deposited Particles Studied by micro-FT-IR Spectroscopy and Complementary Methods of Particle Analysis, Anal. Chem., 80, 633–642, 2008.
Lu, P.-D., Wang, F., Zhao, L.-J., Li, W.-X., Li, X.-H., Dong, J.-L., Zhang, Y.-H., and Lu, G.-Q.: Molecular events in deliquescence and efflorescence phase transitions of sodium nitrate particles studied by Fourier transform infrared attenuated total reflection spectroscopy, J. Chem. Phys., 129, 104509, doi:10.1063/1.2973623, 2008.
Martin, S. T.: Phase Transitions of Aqueous Atmospheric Particles, Chem. Rev., 100, 3403–3453, 2000.
Mikhailov, E., Vlasenko, S., Martin, S. T., Koop, T., and Pöschl, U.: Amorphous and crystalline aerosol particles interacting with water vapor: conceptual framework and experimental evidence for restructuring, phase transitions and kinetic limitations, Atmos. Chem. Phys., 9, 9491–9522, doi:10.5194/acp-9-9491-2009, 2009.
Pant, A., Parsons, M. T., and Bertram, A. K.: Crystallization of Aqueous Ammonium Sulfate Particles Internally Mixed with Soot and Kaolinite: Crystallization Relative Humidities and Nucleation Rates, J. Phys. Chem. A, 110, 8701–8709, 2006.
Song, Y.-C., Ryu, J., Malek, M. A., Jung, H.-J., and Ro, C.-U.: Chemical Speciation of Individual Airborne Particles by the Combined Use of Quantitative Energy-Dispersive Electron Probe X-ray Microanalysis and Attenuated Total Reflection Fourier Transform-Infrared Imaging Techniques, Anal. Chem., 82, 7987–7998, 2010.
Tang, I. N.: Chemical and size effects of hygroscopic aerosols on light scattering coefficients, J. Geophys. Res., 101, 19245–19250, 1996.
Tang, I. N. and Fung, K. H.: Hydration and Raman scattering studies of levitated microparticles: $Ba(NO_3)_2$, $Sr(NO_3)_2$, and $Ca(NO_3)_2$, J. Chem. Phys., 106, 1653–1660, 1997.
Tang, I. N. and Munkelwitz, H. R.: Water activities, densities, and refractive indices of aqueous sulfates and sodium nitrate droplets of atmospheric importance, J. Geophys. Res., 99, 18801–18808, 1994.
Tang, I. N., Tridico, A. C., and Fung, K. H.: Thermodynamic and optical properties of sea salt aerosols, J. Geophys. Res., 102, 23269–23275, 1997.

ACPD
11, 23203–23229, 2011

Ten Brink, H. M.: Reactive uptake of HNO_3 and H_2SO_4 in sea-salt (NaCl) particles, J. Aerosol Sci., 29, 57–64, 1998.
Weingartner, E., Gysel, M., and Baltensperger, U.: Hygroscopicity of Aerosol Particles at Low Temperatures. 1. New Low-Temperature H-TDMA Instrument: Setup and First Applications, Environ. Sci. Technol., 36, 55–62, 2002.

ACPD
11, 23203–23229, 2011

Table 1. Encountering probability of $NaNO_3$ particles of types 1–3 for 9 experimental cases.

Experimental set-ups	Case 1	Case 2	Case 3	Case 4	Case 5	Case 6	Case 7	Case 8	Case 9
Sample	Particles generated by nebulization of DI water solution with N_2 gas	Powder	Powder	Particles kept in a desiccator	Oven-dried aerosols	Particles generated by nebulization of tap water solution with ambient air	Particles generated by nebulization of DI water solution with N_2 gas	Particles generated by nebulization of DI water solution with N_2 gas	Particles generated by nebulization of DI water solution with N_2 gas
$NaNO_3$ purity	99.999 %	99.999 %	98 %	99.999 %	99.999 %	99.999 %	98 %	99.999 %	99.999 %
Collecting substrate	TEM grid	TEM grid	TEM grid	TEM grid	TEM grid	TEM grid	TEM grid	Al foil	Ag foil
Number of angular particles	16 (4.5 %)	47 (100 %)	82 (100 %)	11 (8.7 %)	9 (6.5 %)	10 (7.3 %)	16 (7.1 %)	37 (28.5 %)	116 (95.9 %)
Number of Type 1 particles (no DRH and ERH)	334 (93.3 %)	–	–	48 (37.8 %)	9 (6.5 %)	122 (89.1 %)	207 (92.4 %)	77 (59.2 %)	–
Number of Type 2 particles (only 1st DRH)	20 (5.6 %)	–	–	79 (62.2 %)	119 (86.2 %)	6 (4.5 %)	9 (4.0 %)	26 (20.0 %)	10 (8.3 %)
Number of Type 3 particles (reproducible DRH and ERH)	4 (1.1 %)	47 (100 %)	82 (100 %)	–	10 (7.3 %)	9 (6.6 %)	8 (3.6 %)	27 (20.8 %)	111 (91.7 %)
Overall number of particles	358 (100 %)	47 (100 %)	82 (100 %)	127 (100 %)	138 (100 %)	137 (100 %)	224 (100 %)	130 (100 %)	121 (100 %)

ACPD
11, 23203–23229, 2011

Table 2. The measured DRHs and ERHs of $NaNO_3$ particles for 9 experimental cases.

Experimental set-ups		Case 1	Case 2	Case 3	Case 4	Case 5	Case 6	Case 7	Case 8	Case 9
Sample		Particles generated by nebulization of DI water solution with N_2 gas	Powder	Powder	Particles kept in a desiccator	Oven-dried aerosols	Particles generated by nebulization of tap water solution with ambient air	Particles generated by nebulization of DI water solution with N_2 gas	Particles generated by nebulization of DI water solution with N_2 gas	Particles generated by nebulization of DI water solution with N_2 gas
$NaNO_3$ purity		99.999 %	99.999 %	98 %	99.999 %	99.999 %	99.999 %	98 %	99.999 %	99.999 %
Collecting substrate		TEM grid	TEM grid	TEM grid	TEM grid	TEM grid	TEM grid	TEM grid	Al foil	Ag foil
1st cycle	DRH (%)	73.8±0.1	74.0±0.2	73.8±0.2	74.5±0.3	74.4±0.2	73.6±0.4	73.4±0.2	74.3±0.2	74.1±0.3
	ERH(%)	26.6–18.5	45.3–28.0	47.1–34.3	–	29.9–13.7	36.1–20.1	29.8–15.0	55.2–14.5	65.1–13.5
2nd cycle	DRH(%)	73.5±0.1	74.0±0.2	73.6±0.1	–	74.5±0.1	73.4±0.3	73.6±0.1	74.3±0.2	74.1±0.2
	ERH(%)	25.8–18.9	45.7–26.7	46.5–33.9	–	28.3–13.5	37.2–20.9	28.7–16.3	52.8–12.9	64.3–10.8

ACPD
11, 23203–23229, 2011

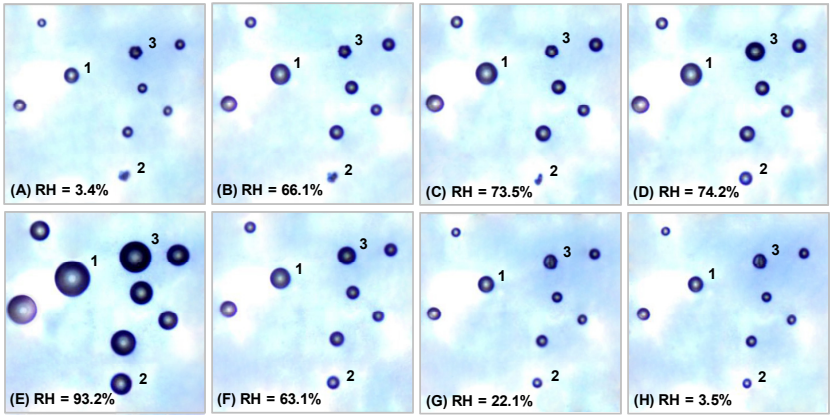

Fig. 1. Optical images of generated $NaNO_3$ particles obtained at **(A)**–**(E)** RH = 3.4 %, 66.1 %, 73.5 %, 74.2 %, and 93.2 % during the humidifying process and at **(F)**–**(H)** RH = 63.1 %, 22.1 %, and 3.5 % during the dehydration process.

ACPD
11, 23203–23229, 2011

Hygroscopic behavior of individual $NaNO_3$ particles

M.-J. Lee et al.

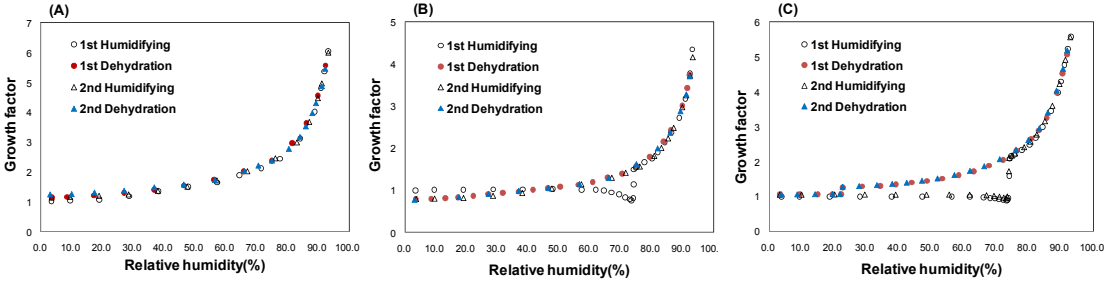

Fig. 2. Humidifying and dehydration curves for generated $NaNO_3$ particles collected on a TEM grid: **(A)**–**(C)** for particle numbers 1–3 in Fig. 1, respectively. Blanks and solids are growth factor data obtained during the humidifying and dehydration processes.

ACPD
11, 23203–23229, 2011

Hygroscopic behavior of individual $NaNO_3$ particles

M.-J. Lee et al.

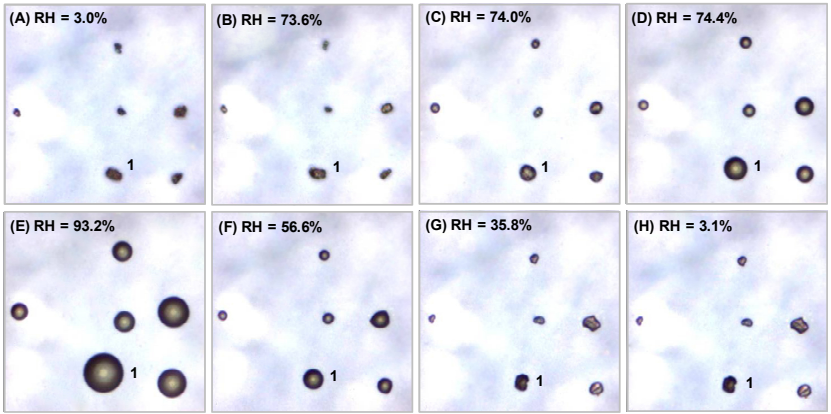

Fig. 3. Typical optical images of $NaNO_3$ powdery particles obtained at **(A)**–**(E)** RH = 3.0 %, 73.6 %, 74.0 %, 74.4 %, and 93.2 % during the humidifying process and at **(F)**–**(H)** RH = 56.6 %, 35.8 %, and 3.1 % during the dehydration process.

ACPD
11, 23203–23229, 2011

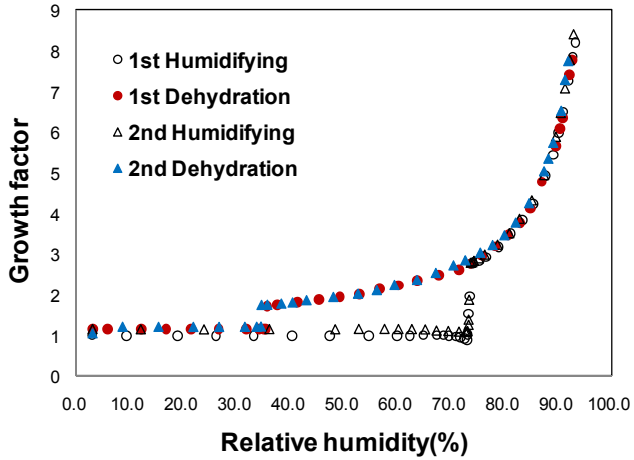

Fig. 4. Humidifying and dehydration curves for a typical $NaNO_3$ powdery particle collected on a TEM grid for particle #1 in Fig. 3. Blanks and solids are growth factor data obtained during the humidifying and dehydration processes.

ACPD
11, 23203–23229, 2011

Hygroscopic behavior of individual $NaNO_3$ particles

M.-J. Lee et al.

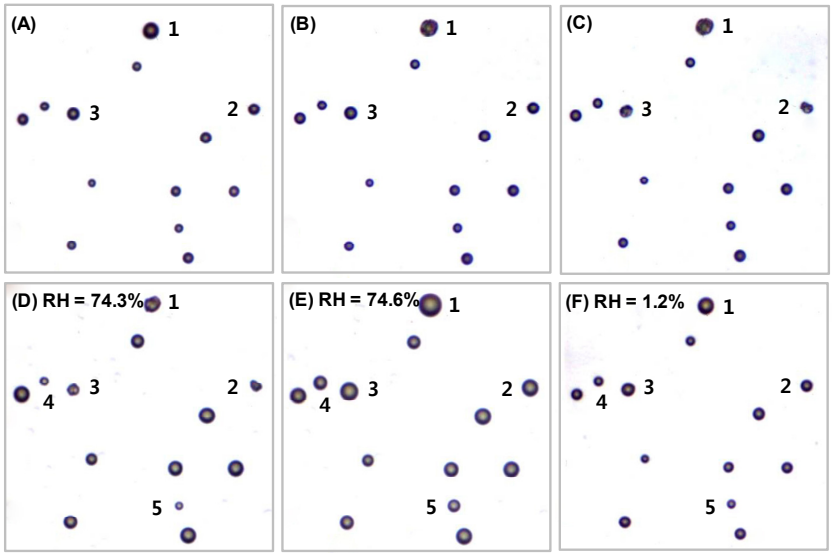

Fig. 5. Optical images of the generated round $NaNO_3$ aerosols on a TEM grid **(A)** that were put in a vacuum desiccator where RH = 15 % and that stayed in the vacuum desiccator **(B)** for 3 days and **(C)** for 13 days. Optical images obtained at **(D)**–**(F)** RH = 74.3 % and 74.6 %, during the humidifying process and 1.2 % during the dehydration process performed for particles that had stayed in the vacuum desiccator for 27 days.

ACPD
11, 23203–23229, 2011

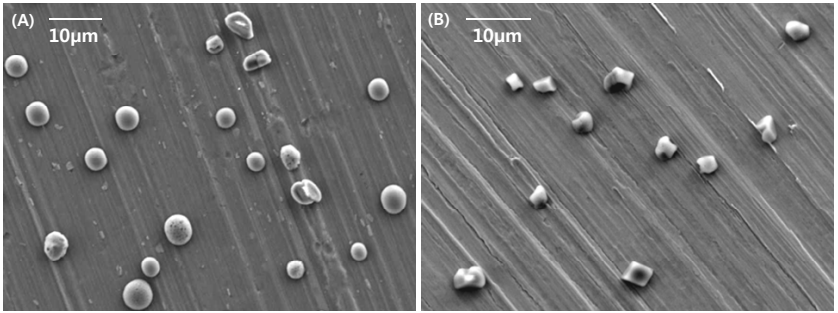

Fig. 6. SEIs of $NaNO_3$ aerosol particles collected on **(A)** Al foil and **(B)** Ag foil.

ACPD
11, 23203–23229, 2011